Impact of the altimeter orbit on the reproduction of oceanic rings: application to a regional model of the Gulf Stream

Oceanic eddies
Altimeter orbit
Objective analysis

Tourbillons océaniques
Altimètre
Orbite
Analyse objective

Eric P. CHASSIGNET [a], William R. HOLLAND [b], Antonietta CAPOTONDI [b]

[a] RSMAS/MPO, University of Miami, 4600 Rickenbacker Causeway, Miami, Florida 33149-1098, USA.

[b] National Center for Atmospheric Research, P.O. Box 3000, Boulder, Colorado 80307-3000, USA.

ABSTRACT

The impact of three altimeter sampling patterns (Geosat, ERS-1 and Topex-Poseidon) on the estimation of mesoscale eddy sea surface height anomalies is investigated in detail by making use of a regional model of the Gulf Stream and of an objective analysis. It is shown that, in a domain-averaged statistical sense, track sequencing does not appear to be of importance in the eddy field recovery. On the other hand, significant differences appear when one starts to look at specific processes such as rings. Qualitatively speaking, the manner in which a ring's signature is represented depends strongly upon the altimeter orbit choice. A higher space sampling such as ERS-1 is preferable in order to keep track of a ring, but to the detriment of its amplitude. A low space sampling (or high time sampling) such as Topex-Poseidon does not provide enough information and the ring's signature vanishes from the resulting maps.

Oceanologica Acta, 1992. **15**, 5, 479-490.

RÉSUMÉ

Impact des données d'altimétrie satellitaire sur la reproduction du champ tourbillonnaire océanique : application à un modèle régional du Gulf Stream

L'impact de trois orbites correspondant aux altimètres Geosat, ERS-1 et Topex-Poséidon sur la reproduction des tourbillons océaniques est analysée en détail avec un modèle régional du Gulf Stream et une analyse objective. Il est montré que, statistiquement, le choix de l'échantillonnage temporel et spatial est de peu d'importance dans la recréation du champ tourbillonnaire. Par contre, des différences importantes apparaissent au niveau des tourbillons. La façon dont le signal d'un tourbillon est reproduit dépend fortement de l'orbite de l'altimètre. Un échantillonnage de haute densité spatiale tel qu'ERS-1 permet de garder trace du tourbillon. Le cas contraire d'un échantillonnage d'une faible densité spatiale (ou haute densité temporelle) tel que Topex-Poséidon ne fournit pas suffisamment d'informations et le signal du tourbillon disparaît du champ final.

Oceanologica Acta, 1992. **15**, 5, 479-490.

INTRODUCTION

Of particular interest to oceanographers are mesoscale features such as the energetic meanders of intense western boundary currents as they penetrate into the ocean interior, the associated rings that detach from these meanders, and the mesoscale eddies present in the open ocean away from the western boundary. Rings, *i. e.* eddies with a scale of a few hundred kilometers which detach themselves from intense western boundary currents through meander cutoffs, are extremely energetic (Olson, 1991) and are thought to play a significant role in the general oceanic circulation (Holland and Lin, 1975; Holland, 1978). By virtue of their formation process, eddies constitute an efficient mechanism whereby heat, salt and potential vorticity are transferred across frontal zones, which otherwise act as barriers to mixing between different water masses. Observations of sea surface height with a satellite altimeter can be used by oceanographers synoptically to reconstruct mesoscale eddy variability. These maps can then be used to analyse the properties and dynamics of such variability; or they can be assimilated into eddy-resolving ocean general circulation models. Much work already is underway to examine the Geosat dataset and to develop assimilation techniques that can extrapolate surface information into the ocean interior (Verron and Holland, 1989; Holland and Malanotte-Rizzoli, 1989; White *et al.*, 1990; Verron, 1990; Haines, 1991; Mellor and Ezer, 1991).

Unfortunately, the sampling patterns of altimeter satellites limit the range of space and time scales of the mesoscale variability field that can be resolved. These sampling patterns involve a trade-off between spatial and temporal resolution, and there is at present no consensus on which compromise provides the best possible representation of mesoscale variability (Wunsch, 1989). Two orbital parameters (dependent upon each other) are particularly important in determining the space and time scales that can be resolved: the repeat period (the period in which a global coverage will be achieved); and the resolution (the spacing between individual tracks and crossover points). In the next few years, the oceanographic community will have at its disposal several altimeter datasets such as Geosat (1986-1989), ERS-1 (1991) and Topex-Poseidon (1992). These satellites will have a repeat period of 17, 35 and 10 days, and a corresponding track spacing of about 140, 80 and 270 km at 37.5° N, respectively. Consequently, they will not resolve the same range of space and time scales. In particular, each altimeter will map the mesoscale eddies synoptically in a different manner. Another point to be noted is that ERS-1 and Topex-Poseidon will most probably sample the ocean surface simultaneously.

In the present paper, by making use of a multi-level model of the Gulf Stream system that has realistic space and time scales of behavior, we inquire into the ability of each altimeter successfully to map the sea surface height anomaly field, one of the primary goals being to document the impact of the altimeter sampling pattern on the estimation of the ring signal. The choice of a regional model of the Gulf Stream as a framework for this study is based on two considerations: 1) the region is extremely active and has many mesoscale eddies; and 2) we have at our disposal a numerical model that compares extremely well with available observations (Holland and Schmitz, 1992).

The layout of the paper is as follows. The model characteristics, altimeter orbits and sampling are first described in the second section. The third section introduces and describes the objective mapping technique. In the fourth one, the ability of each altimeter sampling pattern to match the sea surface height field is examined. Lastly, the results are summarized and discussed in the concluding section.

DESCRIPTION OF THE MODEL, ALTIMETER ORBITS AND SAMPLING

The high-resolution (1/8 degree), regional, quasi-geostrophic (QG) numerical model of the Gulf Stream is configured in a rectangular domain from 80° to 40° W and from 25° to 50° N with five layers in the vertical (layer thicknesses are 300, 450, 750, 1 300 and 2 200 m, respectively). Although wind forcing acts upon the region, the circulation is primarily driven by the specified inflow of the Gulf Stream as a western boundary current south of Cape Hatteras and by the predicted outflow of the stream across the eastern boundary. Topography is included in the bottom layer as are a deep western boundary current inflow and outflow. The numerical model is based upon the closed basin quasi-geostrophic formulation described in Holland (1978), but with the inclusion of open boundary conditions. For more details, the reader is referred to Holland (1978; 1987) and Holland and Schmitz (1992). In the latter, the model parameters are tuned so that the model statistics are brought into accord with observations, to the extent possible. An instantaneous pattern of the total sea surface height is presented in Figure 1.

To investigate the impact of the altimeter orbit on the reproduction of the eddy flow field, the model sea surface

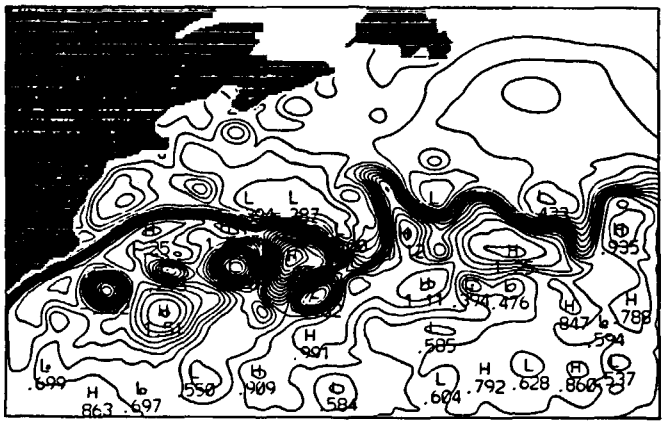

Figure 1

Instantaneous pattern of the total sea surface height for the Gulf Stream regional model (in meters).

Champ instantané de la topographie de surface pour le modèle régional du Gulf Stream (en mètres).

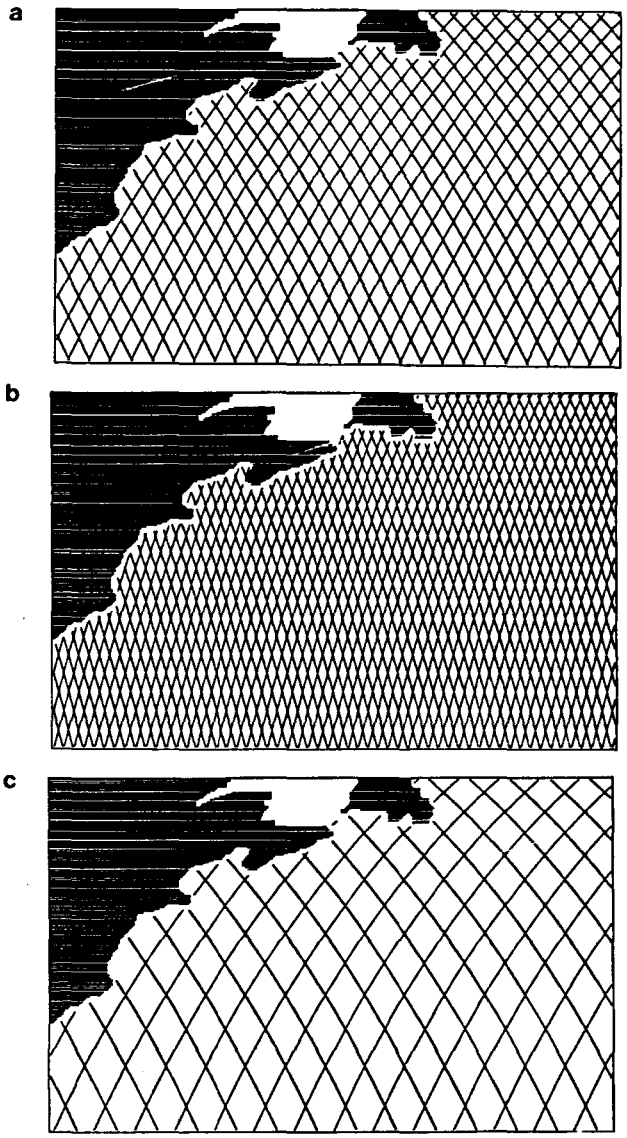

Figure 2

Track coverage of the three satellites over the model domain: a) Geosat; b) ERS-1; and c) Topex-Poseidon.

Couverture des traces correspondant aux trois satellites : a) Geosat ; b) ERS-1 ; et c) Topex-Poséidon.

height, h_s [equivalent to the upper layer streamfunction in the quasi-geostrophic context, $h_s = (f_0/g)\,\psi_1$], was sampled along the tracks of the three satellites (Geosat, ERS-1 and Topex-Poseidon) for a period of two years. The time sampling interval was one second, which approximately corresponds to a data point every 5 km along the track. The sea surface height anomaly is then obtained for each track by removing its two-year mean.

For comparison, the sampling patterns of the three satellites within the model domain are shown in Figure 2 *a*, *b* and *c*. The corresponding spacing between the tracks is approximately 140, 80 and 270 km for Geosat, ERS-1 and Topex-Poseidon, respectively. Of particular interest is ERS-1 which will possess a sub-cycle of sixteen days with a corresponding track separation of about 160 km (not illustrated), meaning that the altimeter will complete a coverage of the earth after one such period, but with coarser spacing. It is then equivalent to say that, for ERS-1, two full coverages of the domain will be at our disposal (at day 16 and 35), shifted by a distance of approximately 80 km.

OBJECTIVE ANALYSIS OF THE DATA

Many methods of interpolating data into a regular grid (referred to as "objective analysis") have been suggested (*see* Gustafsson (1981) for a review). For some considerable time, the preferred method has been the so-called successive correction method, first proposed by Bergthorson and Döös (1955) and expanded by Cressman (1959). More recently, statistical (or optimal) interpolation schemes have been developed on the basis of ideas first introduced by Eliassen (1954) and Gandin (1963), and have been successfully applied to oceanographic situations (Bretherton *et al.*, 1976; De Mey and Robinson, 1987; Mellor and Ezer, 1991; Mariano and Brown, 1992). Statistical interpolation has the advantage that information from different sources may be combined in a manner which pays attention to the reliability of each source. However, successive correction methods are still of interest since: 1) they permit multiple scale analysis; and 2) they can be used when the signal statistics is unknown or highly unhomogeneous. Furthermore, in comparison with the successive correction method, statistical interpolation is expensive in computer time.

The computational cost of solving the system for the statistical interpolation is proportional to the cube of the number of observations allowed to influence a grid point. Most operational statistical interpolation schemes therefore impose severe limitations on this number, with the result that the analysis is not strictly optimal (Bratseth, 1986). The cost of the successive correction method is less sensitive to the number of observations involved. When applied to the Geosat measurements of the Agulhas Current region, the successive correction method, once calibrated, proved to be sixty times faster than the statistical interpolation scheme (Zlotnicki, 1990, pers. comm.). The domain size (10° x 25°) was much smaller than the one used in the present study (25° x 40°) and the difference in computational cost is then even greater in the latter (Bratseth, 1986).

The successive correction method involves the successive modifications of an initial guess field. If we consider the guess field $xg^{(\nu)}{}_s$ defined at each grid point (i, j) on the ν-iterative guess, we can compute the guess field value at each observation location "s" using a 9-point Lagrangian interpolation:

$$xg^{(\nu)}{}_s = \sum_{i=I-1_{j=J-1}}^{i=I+1\,j=J+1} w_{ij}\, xg^{(\nu)}{}_{i,j} \qquad (1)$$

where (I, J) is the closest grid point to the station s and

$$w_{ij} = \prod_{k=I-1_{k\neq i}}^{k=I+1} \frac{(x - x_k)}{(x_I - x_k)} \prod_{l=J-1_{l\neq J}}^{l=J+1} \frac{(y - y_l)}{(y_J - y_l)} \qquad (2)$$

The error $E^{(\nu)}_s$ between the interpolated value $xg^{(\nu)}_s$ and the actual observation x_s (station value) is

$$E^{(\nu)}_s = x_s - xg^{(\nu)}_s \tag{3}$$

The value of the error $E^{(\nu)}_s$ will give a correction to a nearby grid point for the $(\nu + 1)$ iterative value. This correction is given by

$$C^{(\nu+1)}_{ij} = \frac{\sum_s W^{(\nu)}_s E^{(\nu)}_s}{\sum_s W^{(\nu)}_s} \tag{4}$$

where $W^{(\nu)}_s$ is a weighting factor defined as

$$W^{(\nu)}_s = w^{(\nu)}_{ij}(d)\beta \tag{5}$$

Here, $w^{(\nu)}_{ij}(d)$ is the Cressman weighting function at the ν iteration level for the grid point (i, j) and is defined by

$$w^{(\nu)}_{ij}(d) = \begin{cases} R^2_\nu - d^2 & d < R_\nu \\ R^2_\nu + d^2 & d > R_\nu \\ 0 \end{cases} \tag{6}$$

where R_ν is the influence radius and d is the distance of the observation from the grid point. The radius of influence R_ν is a function of the iteration ν and decreases with each scan. The time weighting function β is defined by

$$\beta = e^{-\alpha(\Delta t)^2} \tag{7}$$

where Δt is the time separation of the observation. The next iterative guess is obtained by the formula

$$ug^{(\nu+1)}_{ij} = ug^{(\nu)}_{ij} + aC^{(\nu+1)}_{ij} \tag{8}$$

where a is a smoothing factor which is used to force the resultant field to adjust smoothly to the guess field when approaching data-void areas. Accepting the guess field over data-void areas is believed to be more reliable than extrapolation of distant existing data. The smoothing factor a is defined as

$$a = \begin{cases} 1 & D \le 0.5R_\nu, N > 0 \\ (R_\nu - D)/(0.5R_\nu & D > R_\nu, N > 0 \\ 0 & N = 0 \end{cases}$$

where D is the distance from the grid point (i, j) to the location of the center of gravity of the N influencing stations within the influence radius R_ν.

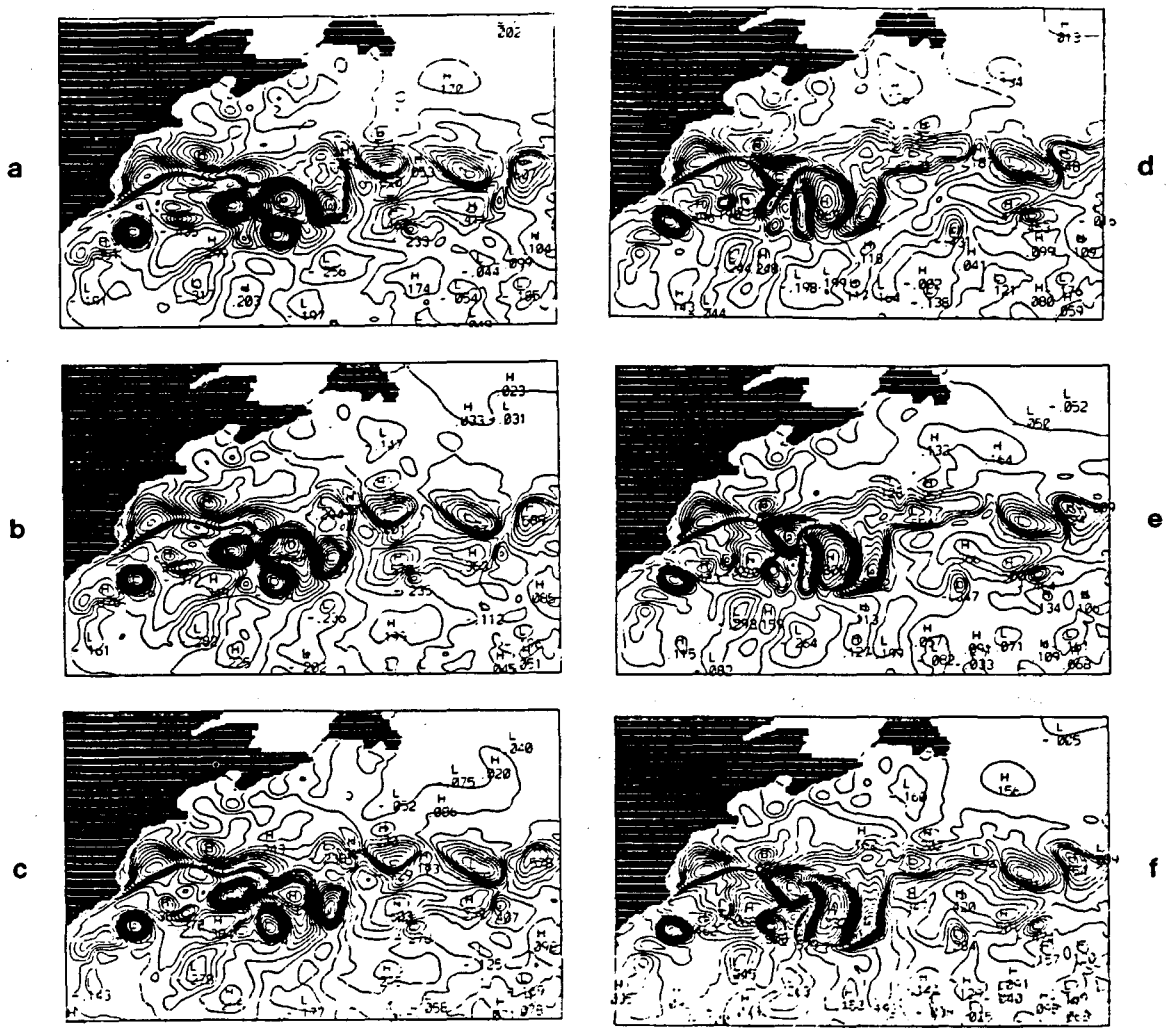

Figure 3

Time evolution of the reference anomaly field from day 34 to 38 of year 5 (a, b, c) and from day 46 to 50 ((d, e, f) (in meters).

Évolution temporelle du champ tourbillonnaire de référence du jour 34 à 38 (a, b, c) et du jour 46 à 50 de la 5ème année d'intégration.

REPRODUCTION OF THE EDDY FIELD

In this section, the datasets corresponding to each altimeter are interpolated to the model grid using the above objective analysis, and maps are created at equal intervals of time. After a qualitative discussion of the ability of each altimeter successfully to reproduce the mesoscale eddy field of the numerical model, the sea surface height interpolated anomaly fields of each satellite being compared to the reference anomaly fields (Fig. 3), the ability of each altimeter to keep track of ring propagation is examined. Finally, the statistics resulting from the interpolation procedure are presented and discussed in order to provide a quantitative measure of each satellite's performance.

Description of the Geosat, ERS-1 and Topex-Poseidon maps

The different weights (in time and space) used in the objective analysis (preceding section) play an important role in the recovery of the eddy field. One has therefore to make a judicious choice of the time weighting function β, of the time window W (in which data are taken into account), and of the different radii of influence R_V. An extensive study was performed to investigate the influence of the latter parameters. In carrying out the analysis, a total of four to six correcting passes through the field were taken with different radii of influence. In Figure 4, five interpolated maps obtained with different β, W and R_V from the Geosat dataset are presented and the corresponding parameters are displayed in Table 1. Large time windows (W and e-folding time for β) provide more data points, but, when combined with large radii (R_V), have then the tendency to produce a smooth field (Fig. 4 *e*). On the other hand, when combined with small radii (R_V), the small scale features (Fig. 4 *f*) are overemphasized. The other combinations (Fig. 4 *b*, *c* and *d*) provide a reasonably good balance between smoothness and signal intensity. Finally, an addition of two passes with smaller radii (Fig. 4 *d*) did not improve the interpolated field (in comparison to Fig. 4 *b*).

In the following discussion, only two sets of parameters are retained for the comparison (smoothness *versus* signal

Figure 4

a) reference anomaly field at day 20; b-f) interpolated anomaly fields for Geosat using the parameters displayed in Table 1, respectively (in meters).

a) champ tourbillonnaire de référence au jour 20 ; et b-f) champs tourbillonnaires interpolés pour Geosat avec les paramètres du tableau 1, respectivement (en mètres).

Table 1

Parameter study of the successive correction method.

Analyse paramétrique de la méthode à corrections successives.

Figure 4	W (in days)	*e*-folding time for β (in days)	R_v (in 1/8 degree)
b	10	5	16, 12, 8, 4
c	10	5	20, 16, 12, 8
d	10	5	20, 16, 12, 8, 4, 2
e	20	5	20, 16, 12, 8
f	20	10	20, 16, 12, 8

intensity) and their influence on the reproduction of the eddy field is then presented in relation to each satellite orbit. The chosen parameters are displayed in Table 2.

Geosat

Figures 4 and 5 display the time evolution of series G1 and G2 respectively for a period of ten days. In G1, a small time

Table 2

Parameters for the objective analysis method. The e-folding time for the Gaussian function β is five days for all interpolated maps.

Paramètres de l'analyse objective. L'échelle de temps pour la fonction gaussienne β est de cinq jours pour toutes les cartes.

Experiment	W (in days)	R_v (in 1/8 degree)-
Geosat (G1)	10	16, 12, 8, 4
Geosat (G2)	20	20, 16, 12, 8
ERS-1 (E1)	10	16, 12, 8, 4
ERS-1 (E2)	20	20, 16, 12, 8
Topex-Poseidon	20	20, 16, 12, 8
ERS-1 + Topex-Poseidon	10	20, 16, 12, 8

window (W) and small radii [R_v (Tab. 2)] produce a field with high amplitude features and small scale structures. A wider time window and larger radii in G2 have the tendency to smooth the eddy field to the detriment of the signal's amplitude. Both are able to capture most of the proeminent features of the reference field (Fig. 3), except for the inten-

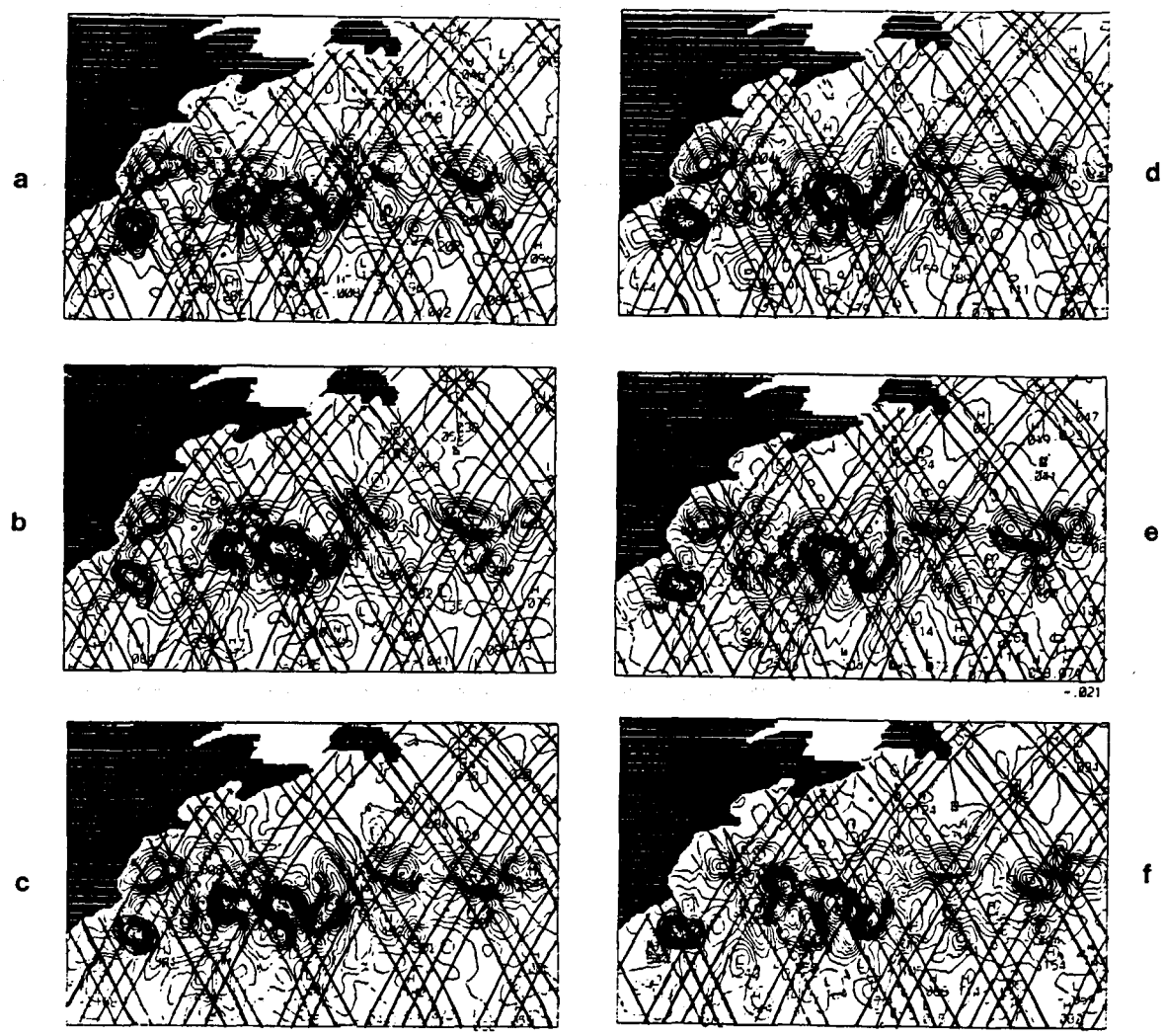

Figure 5

Time evolution G1 (small time window and radii) of the interpolated anomaly field for Geosat from day 34 to 44 (in meters).

Évolution temporelle des champs tourbillonnaires G1 pour Geosat du jour 34 à 44 (en mètres).

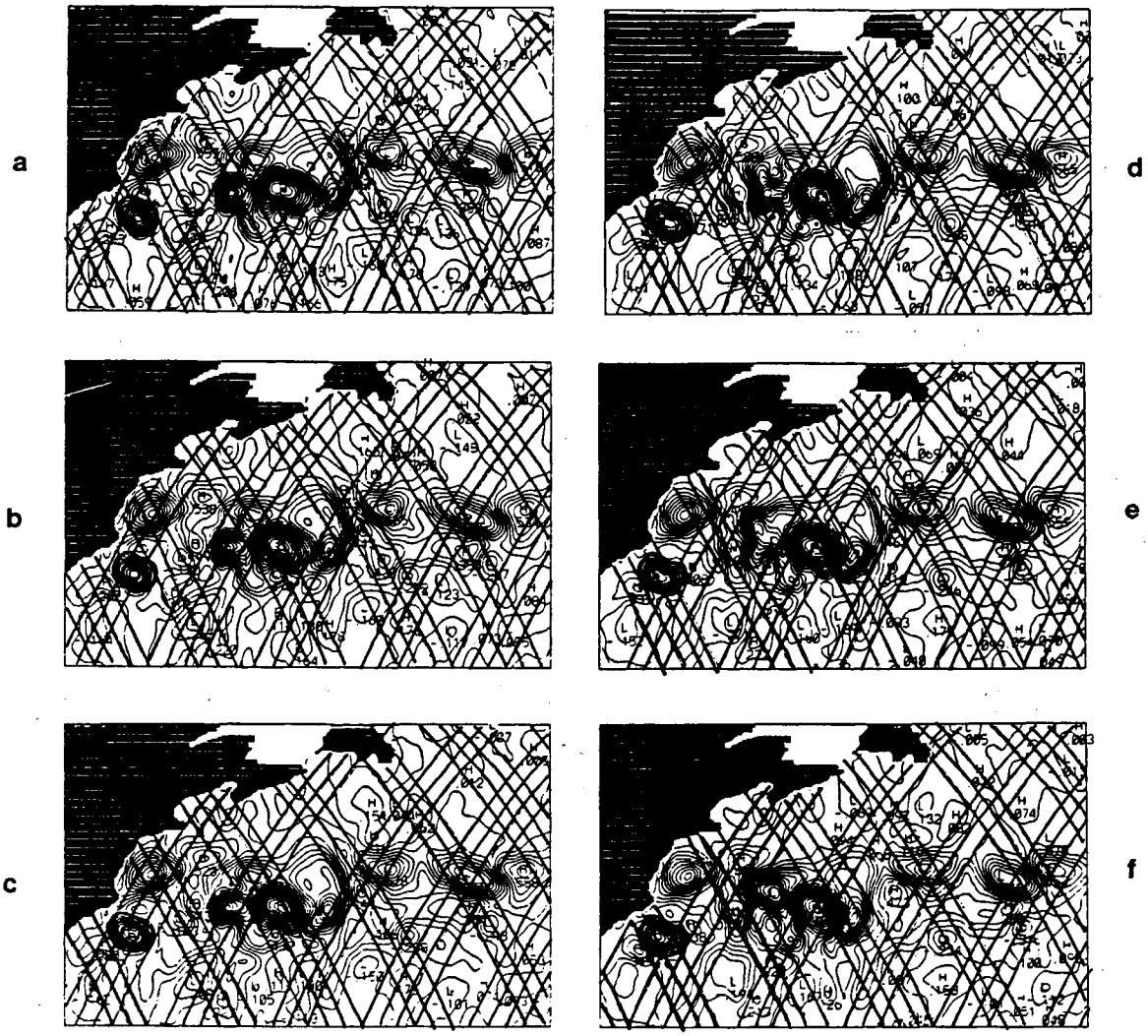

Figure 6

Time evolution G2 (large time window and radii) of the interpolated anomaly field for Geosat from day 34 to 44 (in meters).

Évolution temporelle des champs tourbillonnaires G2 pour Geosat du jour 34 à 44 (en mètres).

sity of the front's signature associated with the Gulf Stream path. Superimposed on the interpolated maps are the Geosat tracks that were given the maximum weight during the objective analysis. They correspond for both G1 and G2 to a period of ten days centered on the time of the analysis. In G1, only data along those tracks contribute to the analysis because of the time window chosen. In G2, maximum weight is given to the data along these tracks, but an additional ten days of data with smaller weight are also taken into account to produce the final map. As a consequence, the highs and lows of the resulting field for G1 are located on the tracks, and the shadow zones in between have little or no information. More data are taken into account in G2 and the final eddy field possesses more information in the so-called shadow zones. There is therefore a trade-off between the two series of maps, namely high amplitude features *versus* a more complete representation.

This is particularly true when one considers rings, such as that located in the southwest corner of the basin (Fig. 3). In Figure 5 (G1), one can observe the ring moving southwestward and at the same time undergoing significant deformation (in comparison with the reference field). The ring's shape and maximum elevation location appear to be a function of the track sampling (Fig. 5 *a*, *b*). When the sampling is sufficient (Fig. 5 *c*, *d*), the ring is fairly well represented. As soon as the coverage is not as complete, the ring's shape becomes distorted. In G2 (Fig. 6), the ring's shape is in better agreement with the reference field since more data are taken into account. The negative aspect is that its amplitude is weaker.

ERS-1

The ten-day time series of interpolated maps for E1 and E2 are presented in Figure 7 and 8 for the same time windows and radii of G1 and G2, respectively (Tab. 2). Again, a small time window and small radii emphasize small scale structures in E1. The ERS-1 satellite tracks are, as for Geosat, superimposed on each map for a ten-day period centered on the time of the analysis. There are fewer shadow zones than in Geosat, but they are larger in size. This contributes to the fact that the ring previously discussed for

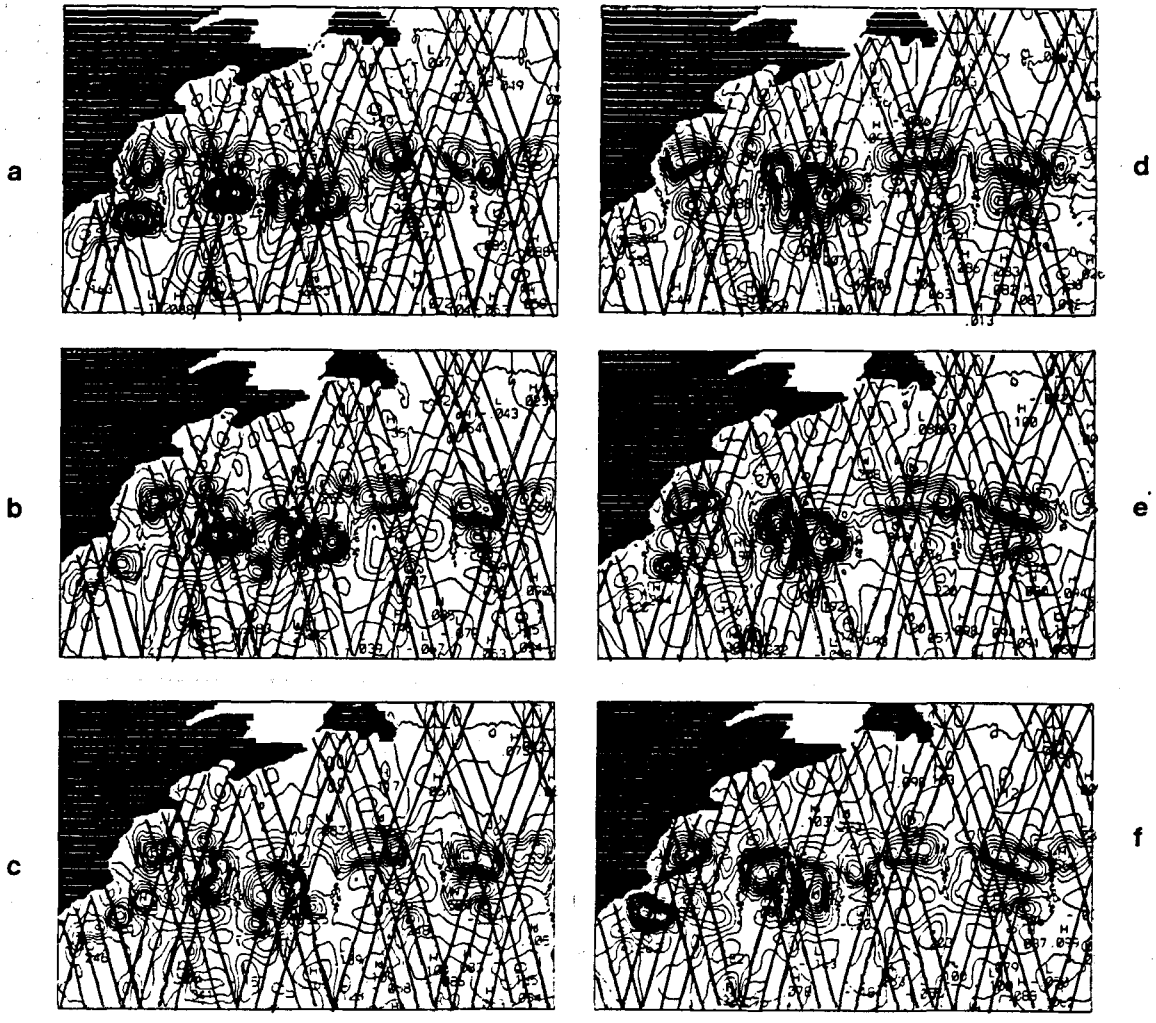

Figure 7

Time evolution E1 (small time window and radii) of the interpolated anomaly field for ERS-1 from day 38 to 48 (in meters).

Évolution temporelle des champs tourbillonnaires E1 pour ERS-1 du jour 38 à 48 (en mètres).

Geosat disappears in Figure 7 *c*, *d*. In the latter (E1), only data along the tracks are taken into account. If one increases the time window as in E2, the ring then becomes present in all maps since more data are taken into account, but, as for Geosat, to the detriment of the ring's amplitude.

Topex-Poseidon

With its full coverage of the domain every ten days, Topex-Poseidon differs substantially from the other two satellites by providing data more frequently, to the detriment of the spatial coverage. A similar eddy field results from both time windows since a large one provides only additional information along the tracks. The impact of such a sampling is illustrated when observing the ring previously discussed for Geosat and ERS-1. In Figure 9, the ring disappears from the interpolated maps. Because the mean ring diameter is of the order of 200 to 300 km for a track separation of 280 km, whenever a ring happens to be located in between tracks (as in Fig. 9 *d*), little or no information about the ring is then provided to the objective mapping routine. In ten days, the ring travels some 50 to 80 km and the previous (or subsequent) track coverage only samples the ring's edge. As a consequence, even when a large window is chosen, because of the small weight given to data outside the ten-day period, the resulting field is not improved over a small window.

ERS-1 + Topex-Poseidon

Taking advantage of the fact that ERS-1 and Topex-Poseidon might sample the ocean surface simultaneously, interpolated maps were also performed from the combined datasets (not illustrated). Overall, the eddy field is better represented, since more data are taken into account. However, it does also happen that, when a large shadow zone of ERS-1 overlaps a ring located between two tracks of Topex-Poseidon as in Figure 9 *d*, the corresponding sea surface signature vanishes from the interpolated maps when a small time window is used. Again, as in ERS-1, if one increases the time window, the ring then becomes present in all maps, but to the detriment of the ring's amplitude.

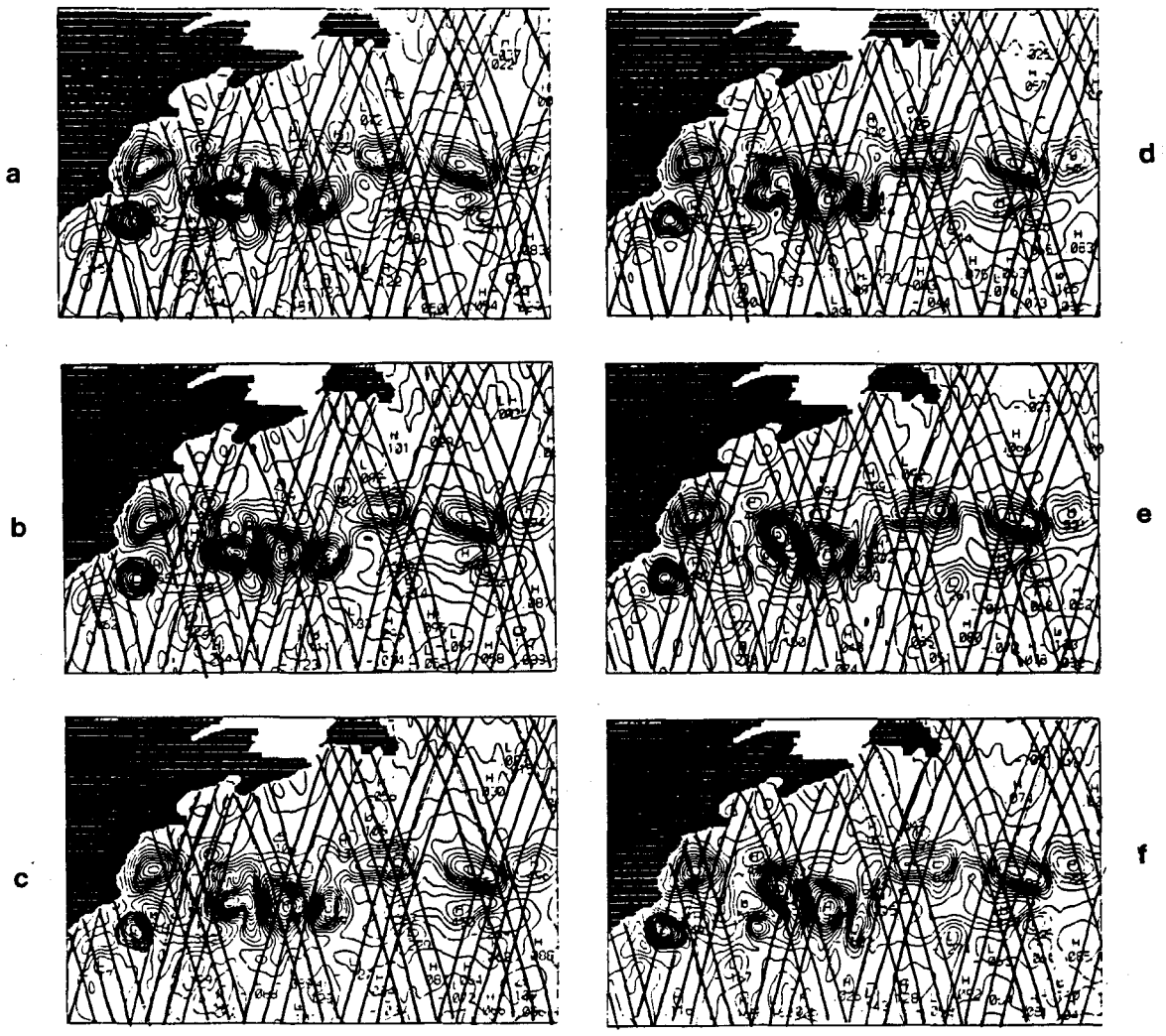

Figure 8

Time evolution E2 (large time window and radii) of the interpolated anomaly field for ERS-1 from day 38 to 48 (in meters).

Évolution temporelle des champs tourbillonnaires E2 pour ERS-1 du jour 38 à 48 (en mètres).

RING TRACKING AND PROPAGATION

In this section, the ability of each altimeter to keep track of the ring discussed in the first part is further investigated. The locations for the ring center (defined as the point of maximum interface displacement) for a thirty-day period are displayed in Figure 10 for the reference field and for four interpolated fields (Geosat, ERS-1, Topex-Poseidon and ERS-1 + Topex-Poseidon).

The large differences observed in the ring locations (Fig. 10) illustrate the impact of the sampling patterns.

A) In the case of Geosat (G2), the ring propagated only about 90 km in the seventeen-day repeat period for a distance between tracks of 140 km. This results in the ring being first observed to remain near a descending track, until it moves sufficiently westward to provide a signal to the closest ascending track. At this point, the ring center jumps westward (Fig. 10 *b*).

B) For ERS-1, in the case of a large window (E2) (and therefore a continuous ring signature), the observed propagation is relatively smooth (Fig. 10 *c*).

C) On the other hand, as expected from the discussion in the first part of the present section, Topex-Poseidon keeps the ring on one track until the ring moves far enough westward to provide information to the adjacent track (Fig. 10 *d*). Since the ring propagated only about 60 km in the ten-day repeat period for a distance between tracks of 270 km, the resulting jump is even greater than in Geosat.

D) When the information from ERS-1 is combined with Topex-Poseidon, more data are taken into account, and the ring propagation is in good agreement with the reference field as in ERS-1 (Fig. 10 *a*, *c*, *e*).

Statistics

The foregoing paragraphs discussed the reproduction of the mesoscale eddy field in a qualitative manner and did not provide a quantitative measure of the orbit's performance. Consequently, 640-day time series for the domain-averaged rms error between the reference field and the interpolated fields were computed for the three altimeters and are presented in Figure 11. The rms errors are all of the same

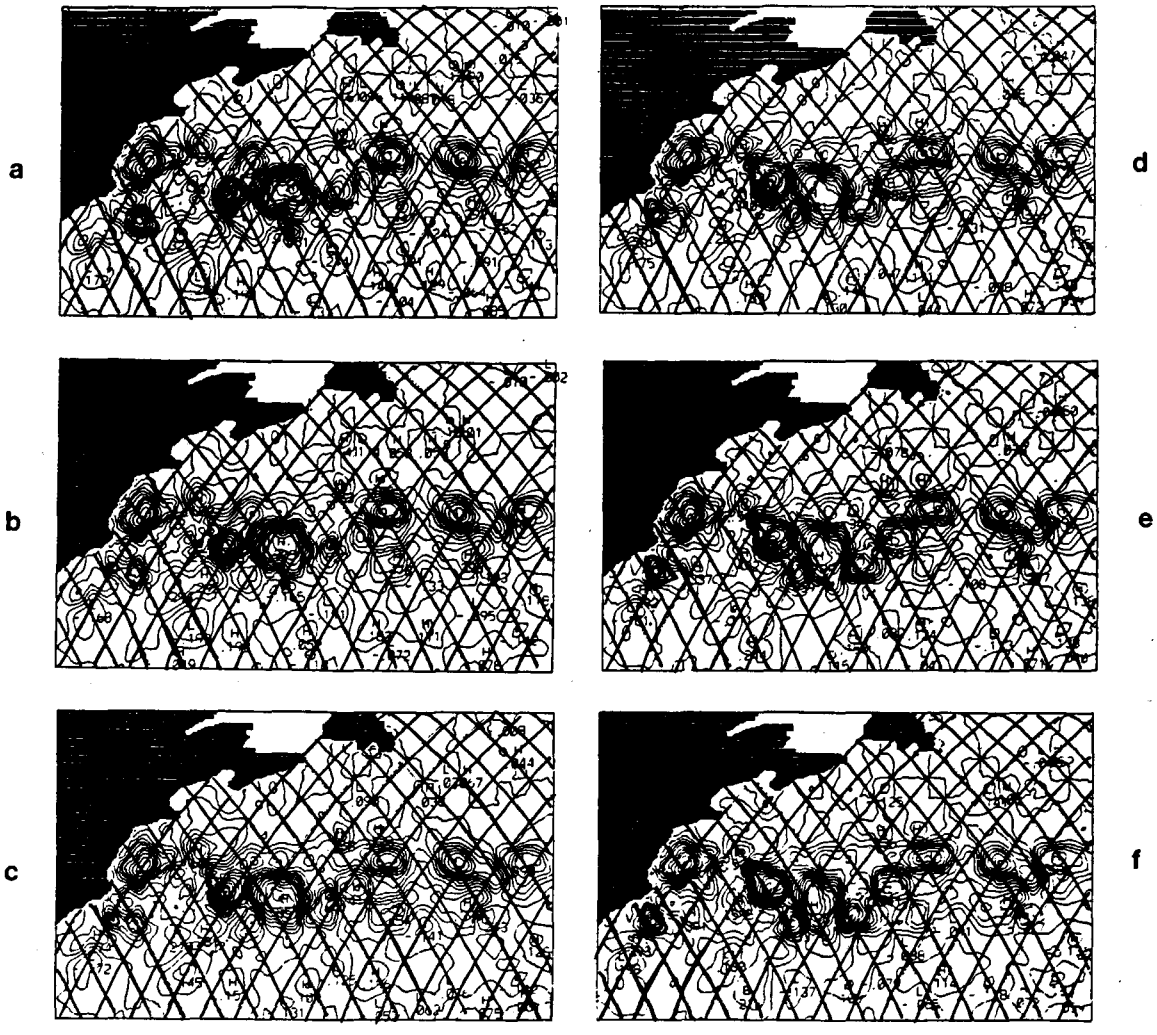

Figure 9

Time evolution of the interpolated anomaly field for Topex-Poseidon from day 34 to 44 (in meters).

Évolution temporelle des champs tourbillonnaires pour Topex-Poséidon du jour 34 à 44 (en mètres).

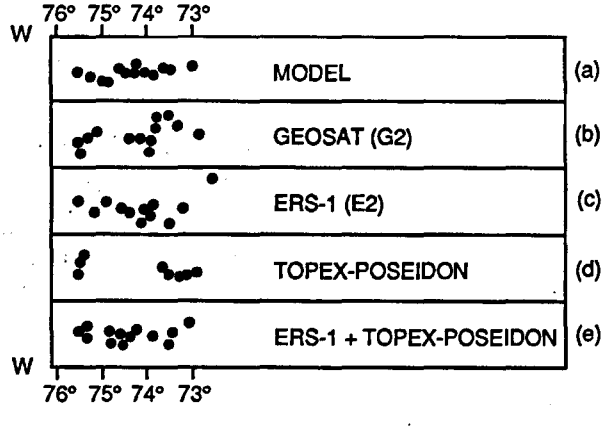

Figure 10

Location of the ring center from day 20 to day 50 (starting from the right) for: a) the reference field; b) Geosat (G2); c) ERS-1 (E2); d) Topex-Poseidon; and e) ERS-1 + Topex-Poseidon.

Situation du centre de l'anneau du jour 20 à 50 (en partant de la droite) pour : a) le champ de référence ; b) Geosat (G2) ; c) ERS-1 (E2) ; d) Topex-Poséidon; et e) ERS-1 + Topex-Poséidon.

order of magnitude (about 50 % of the signal rms) and no significant differences, except perhaps for ERS-1 which is located most of the time under Geosat and Topex-Poseidon, can be noticed among either satellites (Fig. 11). When both ERS-1 and Topex-Poseidon are sampling the sea surface simultaneously, the rms errors are, as expected, on the average smaller (Fig. 12) since more data are provided by the sampling pattern.

SUMMARY AND DISCUSSION

The experiments described in this note are aimed at documenting the relative impact of several altimeter sampling patterns on the estimation of the mesoscale eddy sea surface height anomalies. By making use of: 1) a regional quasi-geostrophic numerical model of the Gulf Stream; 2) error-free measurements; and 3) an objective analysis (successive correction method), three altimeter sampling patterns (Geosat, ERS-1 and Topex-Poseidon) were analysed.

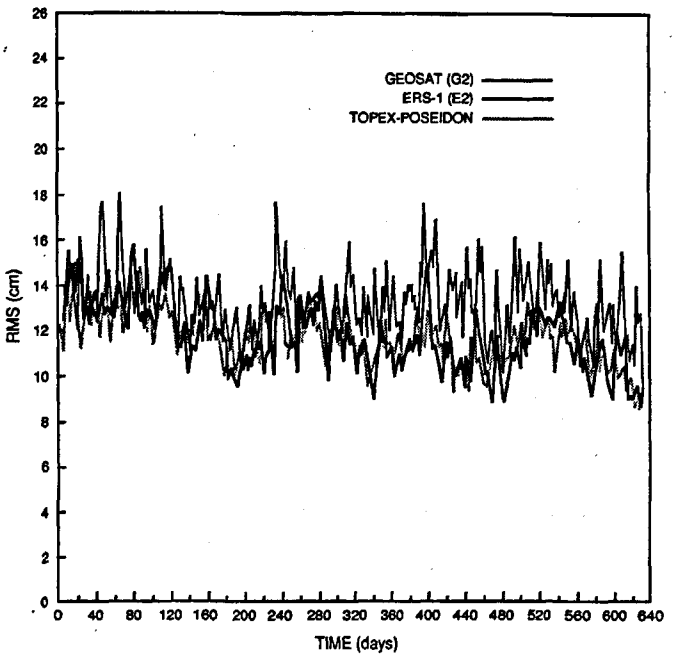

Figure 11

640-day time series of the domain-averaged RMS error between the reference field and the interpolated fields for Geosat (G2), ERS-1 (E2) and Topex-Poseidon.

Série temporelle de 640 jours de la RMS erreur moyenne entre le champ de référence et les champs interpolés de Geosat (G2) ; ERS-1 (E2) ; et Topex-Poséidon.

the way a ring signature is represented in the interpolated maps is strongly dependent upon the altimeter orbit choice. It appears from the fourth section that, in order to keep track of a ring, a higher space sampling like ERS-1 is better, but to the detriment of the amplitude of the interpolated fields. On the other hand, low space sampling (or high time sampling) like Topex-Poseidon does not provide enough information to update the interpolated fields, and the ring's signature vanishes from the resulting maps.

In this paper, special emphasis has been laid on oceanic rings. Other mesoscale processes will have a different signature depending upon the altimeter's orbit choice. One must also bear in mind that this work was performed with an objective analysis which makes use of a successive correction technique. While such an analysis is not optimal because of the parameter choices that are called for, its advantage is that it can be tuned to better represent a specific aspect of the interpolated field, such as, in the case of this study, rings. Other methods which take dynamics into account might be able to provide more and better information. Such work is in progress with the state-of-the-art parameter matrix objective analysis method of Mariano and Brown (1992). Finally, whether this work can be extended to real data depends strongly on factors such as the impact of orbital errors and inconsistencies in frequencies/wavenumbers between the numerical model and the ocean (Wunsch, 1989).

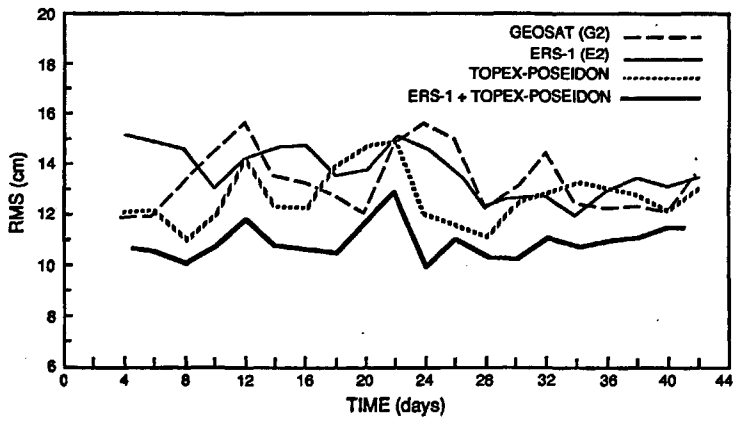

Figure 12

44-day time series of the domain-averaged RMS error between the reference field and the interpolated fields for Geosat (G2), ERS-1 (E2), Topex-Poseidon and ERS-1 + Topex-Poseidon.

Série temporelle de 44 jours de la RMS erreur moyenne entre le champ de référence et les champs interpolés de Geosat (G2) ; ERS-1 (E2) ; Topex-Poséidon et ERS-1 + Topex-Poséidon.

In a quantitative sense, the domain-averaged rms error time series of the interpolated fields are of the same magnitude for the three altimeters. It can therefore be concluded that, statistically, the track sequencing does not appear to be of importance in the eddy field recovery. A similar result was obtained by Holland and Malanotte-Rizzoli (1989) and Verron (1990) when investigating the impact of space *versus* time sampling in the assimilation of altimeter data in ocean circulation models. It was concluded that the detailed track sequencing was not relevant as long as the data space was filled with sufficient regularity. In a statistical sense, the four-dimensional circulation of the ocean was equally well represented.

Significant differences appear when one starts to look at specific processes such as rings. In a qualitative manner,

Acknowledgements

We are indebted to Dr. Zlotnicki for making the successive correction scheme available and for many useful comments during the course of this work. Many thanks to Dr. De Mey for providing the orbit generation package and to J. Chow for her help in producing the different satellite datasets. The authors also whish to thank one anonymous reviewer for an improved manuscript and for pointing out additional advantages of the successive correction method. The computations were carried out using the CRAY computers at the National Center for Atmospheric Research (NCAR). NCAR is sponsored by the National Science Foundation.

REFERENCES

Bergthorsson P. and B.R. Döös (1955). Numerical weather map analysis. *Tellus*, **7**, 329-340.

Bratseth A.M. (1986). Statistical interpolation by means of successive corrections. *Tellus*, **38A**, 439-447.

Bretherton F.P., R.E. Davis and C.B. Fandry (1976). A technique for objective analysis and design of oceanographic experiments applied to MODE-73. *Deep-Sea Res.*, **23**, 559-582.

Cressman G.P. (1959). An operational objective analysis system. *Mon. Weath. Rev.*, **87**, 367-374.

De Mey P. and A.R. Robinson (1987). Simulation and assimilation of satellite altimeter data in the oceanic mesoscale. *J. phys. Oceanogr.*, **17**, 2280-2293.

Eliassen A. (1954). Provisional report on calculation of spatial covariance and autocorrelation of the pressure field, reprinted in: *Data Assimilation Methods*, L. Bengtsson, M. Ghil and E. Kallen, editors. Springer-Verlag, 319-330.

Gandin L.S. (1963). *Objective analysis of meteorological fields.* Hydromet Pres, Leningrad (translated from Russian).

Gustafsson N.A. (1981). A review of methods for objective analysis. in: *Dynamic Meteorology: Data Assimilation Methods.* Springer-Verlag, New York, 36, 17-76.

Haines K. (1991). A direct method for assimilating sea surface height data in ocean models with adjustments to the deep circulation. *J. phys. Oceanogr.*, **21**, 843-868.

Holland W.R. (1978). The role of mesoscale eddies in the general circulation of the ocean - numerical experiments using a wind-drive quasi-geostrophic model. *J. phys. Oceanogr.*, **8**, 363-392.

Holland W.R. (1987). A limited area model for the Gulf Stream region. in: *Three-dimensional Models of Marine and Estuarine Dynamics*, J.C.J. Nihoul and B.M. Jamart, editors. Elsevier Oceanography Series, 45, 127-148.

Holland W.R. and L.B. Lin (1975). On the generation of mesoscale eddies and their contribution to the oceanic general circulation. I: A preliminary numerical experiment. *J. phys. Oceanogr.*, **13**, 1093-1104.

Holland W.R. and P. Malanotte-Rizzoli (1989). Assimilation of altimeter data into an ocean circulation model: space *versus* time resolution studies. *J. phys. Oceanogr.*, **19**, 1507-1534.

Holland W.R. and W.F. Schmitz Jr. (1992). A regional model of the Gulf Stream system (in prep.).

Mariano A.J. and O.B. Brown (1992). Efficient objective analysis of dynamically heterogeneous and nonstationary fields *via* the parameter matrix, *Deep-Sea Res.*, **39**, 1255-1271.

Mellor G.L. and T. Ezer (1991). A Gulf Stream model and an altimetry assimilation scheme. *J. geophys. Res.*, **96**, 8779-8795.

Olson D.B. (1991). Rings in the ocean. *Ann. Rev. Earth planet. Sci.*, **19**, 283-311.

Verron J. (1990). Altimeter data assimilation into an ocean circulation model: sensitivity to orbital parameters. *J. geophys. Res.*, **95**, 11443-11459.

Verron J. and W.R. Holland (1989). Impacts de données d'altimétrie satellitaire sur les simulations numériques des circulations générales océaniques aux latitudes moyennes. *Annls Geophys.*, **7**, 31-46.

White W.B., C.-K. Tai and W.R. Holland (1990). Continuous assimilation of simulated Geosat altimetric sea level into an eddy-resolving numerical ocean model. Part I and II. *J. geophys. Res.*, **95**, 3219-3252.

Wunsch C. (1989). Sampling characteristics of satellite orbits. *J. atmos. ocean. Technol.*, **6**, 891-907.